siRNA incorporated in slow-release injectable hydrogel continuously silences DDIT4 and regulates nucleus pulposus cell pyroptosis through the ROS/TXNIP/NLRP3 axis to alleviate intervertebral disc degeneration

From The Second Clinical Medical College, Lanzhou University, Lanzhou, China

Cite this article:
Bone Joint Res 2024;13(5):
247–260.

DOI: 10.1302/2046-3758.
135.BJR-2023-0320.R1

Correspondence should be sent to Xuewen Kang
ery_kangxw@lzu.edu.cn

M. Ma,[1,2] C. Zhang,[3] Z. Zhong,[4] Y. Wang,[5] X. He,[1,2] D. Zhu,[1,2] Z. Qian,[6] B. Yu,[7] X. Kang[1,2]

[1]The Second Clinical Medical College, Lanzhou University, Lanzhou, China
[2]Department of Orthopaedics, Lanzhou University Second Hospital, Lanzhou, China
[3]Department of Sports Medicine, The Second Affiliated Hospital of Fujian Traditional Chinese Medical University, Fuzhou, China
[4]Department of Orthopaedics, Ruijin Hospital, Shanghai Jiao Tong University, Shanghai, China
[5]Department of Oncology, Zhangye People's Hospital Affiliated to Hexi University, Zhangye, China
[6]Department of Joint and Sports Medicine, Institute of Orthopaedic Diseases, Zhangye People's Hospital Affiliated to Hexi University, Zhangye, China
[7]Shanghai Seventh People's Hospital, Shanghai University of Traditional Chinese Medicine, Shanghai, China

Aims

In this investigation, we administered oxidative stress to nucleus pulposus cells (NPCs), recognized DNA-damage-inducible transcript 4 (DDIT4) as a component in intervertebral disc degeneration (IVDD), and devised a hydrogel capable of conveying small interfering RNA (siRNA) to IVDD.

Methods

An in vitro model for oxidative stress-induced injury in NPCs was developed to elucidate the mechanisms underlying the upregulation of DDIT4 expression, activation of the reactive oxygen species (ROS)-thioredoxin-interacting protein (TXNIP)-NLRP3 signalling pathway, and nucleus pulposus pyroptosis. Furthermore, the mechanism of action of small interfering DDIT4 (siDDIT4) on NPCs in vitro was validated. A triplex hydrogel named siDDIT4@G5-P-HA was created by adsorbing siDDIT4 onto fifth-generation polyamidoamine (PAMAM) dendrimer using van der Waals interactions, and then coating it with hyaluronic acid (HA). In addition, we established a rat puncture IVDD model to decipher the hydrogel's mechanism in IVDD.

Results

A correlation between DDIT4 expression levels and disc degeneration was shown with human nucleus pulposus and needle-punctured rat disc specimens. We confirmed that DDIT4 was responsible for activating the ROS-TXNIP-NLRP3 axis during oxidative stress-induced pyroptosis in rat nucleus pulposus in vitro. Mitochondria were damaged during oxidative stress, and DDIT4 contributed to mitochondrial damage and ROS production. In addition, siDDIT4@G5-P-HA hydrogels showed good delivery activity of siDDIT4 to NPCs. In vitro studies illustrated the potential of the siDDIT4@G5-P-HA hydrogel for alleviating IVDD in rats.

Conclusion

DDIT4 is a key player in mediating pyroptosis and IVDD in NPCs through the ROS-TXNIP-NLRP3 axis. Additionally, siDDIT4@G5-P-HA hydrogel has been found to relieve IVDD in rats. Our research offers an innovative treatment option for IVDD.

Bone & Joint Research

Article focus

- What are the functions and pathways of DNA-damage-inducible transcript 4 (DDIT4) in intervertebral disc degeneration (IVDD)?
- Can hydrogels be synthesized for carrying small interfering RNA (siRNA) and ameliorating IVDD in vivo?

Key messages

- DDIT4 regulates pyroptosis of nucleus pulposus cells via the reactive oxygen species (ROS)-thioredoxin-interacting protein (TXNIP)-NLRP3 axis.
- The use of siDDIT4@G5-P-HA hydrogel demonstrated amelioration of IVDD.

Strengths and limitations

- This study identified DDIT4 as a potential therapeutic target for IVDD.
- This study did not investigate the enduring impacts of polyamidoamine (PAMAM) hydrogel on nucleus pulposus cells.

Introduction

Low back pain (LBP) affects a large proportion of the population worldwide, with approximately 80% of individuals experiencing it at some point in their lives.[1] It imposes a serious socioeconomic burden, and the cost of its management is rapidly increasing with the ageing global population.[2,3] The primary cause of LBP is intervertebral disc degeneration (IVDD).[4,5] The human intervertebral disc consists of cartilage endplates (EP), annulus fibrosus (AF), and nucleus pulposus (NP) at its centre.[6] NPCs maintain the internal environment of the intervertebral disc by synthesizing the extracellular matrix (ECM). The degradation of the ECM and a reduction in the number of NP cells (NPCs) are considered signs of IVDD.[7] The pathogenesis of IVDD is complex and its pathogenesis remains elusive. Changes in the microenvironment of the NP play a decisive and harmful role in the pathogenesis of IVDD.[8] The initiation of IVDD involves multiple factors, among which oxidative stress plays an important role. Some studies have demonstrated that disc degeneration is associated with reactive oxygen species (ROS);[9] however, the specific mechanisms underlying oxidative stress-induced pyroptosis of NPCs warrant further investigation.

DNA damage-inducible transcript 4 (DDIT4) is an evolutionarily conserved protein that has low expression under basal conditions, but is overexpressed when cells are stimulated by oxidative stress, endoplasmic reticulum stress, and hypoxia.[10,11] Subsequent independent studies have reported that DDIT4 is involved in various diseases, including Alzheimer's disease and Parkinson's disease,[12] myocardial ischaemia/reperfusion injury,[13] and osteoarthritis.[14] Nevertheless, the role of DDIT4 in IVDD warrants further exploration.

Small interfering RNAs (siRNAs) have been identified as mediators of RNA interference (RNAi) in mammalian cells,[15] and can efficiently and specifically target mRNAs.[16] Based on these characteristics, siRNA-based treatment represents a promising approach to treating IVDD.[17,18] Research on the role and application value of siRNA-based drugs is expanding, owing to their good record of safety, specificity, and high efficiency. However, siRNAs have a short half-life, can be degraded by nucleases and readily cleared from blood circulation, and require special transfection reagents to enter cells because of their negative charge.[19–21] Moreover, the cytotoxicity and transfection efficiency of transfection reagents require additional considerations. Therefore, the key to enhancing the therapeutic potential of siRNAs is to develop a carrier with improved delivery efficiency.

In recent years, non-viral vectors, including cationic liposomes and polymers, have been widely used for siRNA transfection.[22] Polyamidoamine (PAMAM) is a new class of synthetic polymer that has a highly ordered 3D backbone with multiple terminals and a dendrite-like shape.[23] They comprise three components, namely a central core, the branched chains, and the terminal groups.[24] The branched chains stem from the central core, and their repetition results in the formation of spherical or circular structures called generations (G) and the branched chains form 'gaps' between them.[25] PAMAM contains multiple terminal groups that determine the polarity of PAMAM. For instance, the terminal amino group can confer the molecule with a positive charge.[26] The protonation of the terminal amino group makes PAMAM positively charged, and the internal 'gaps' potentially adsorb negatively charged siRNAs. Therefore, the combination of PAMAM and siRNAs represents a novel strategy for the treatment of IVDD.

Methods

Human intervertebral disc tissue collection, ethics approval, and consent to participate

Human intervertebral disc tissues were selected from patients with varying degrees of degeneration (n = 6, Table I) based on the Pfirrmann grading of MRI examinations.[27] The tissues were classified as mildly degenerated (MDD, Pfirrmann grading I and II) or severely degenerated (SDD, Pfirrmann grading III, IV, and V). The intervertebral discs in the MDD group were obtained from patients with congenital scoliosis, while those in the SDD group were obtained from patients with herniated discs. The study was performed in accordance with the 1964 Declaration of Helsinki and subsequent versions,[28] and was approved by The Human Ethics Committee of Lanzhou University Second Hospital (2023A-105) and The Animal Ethics Committee of the Lanzhou University Second Hospital (D2023-145). All enrolled patients provided written informed consent and all animal experiments were conducted in accordance with the National Institutes of Health (NIH, USA) Guide for the Care and Use of Laboratory.

Extraction of rat nucleus pulposus cells

Primary rat NPCs were isolated using a method described by He et al.[29] Tissues from four rats (eight-week-old Sprague-Dawley rats, weight 200 g (± 20 g)) were mixed and digested with 0.25% trypsin at 37°C for 30 minutes. Mixture of tissues and trypsin was blown with a pipette every ten minutes until the nucleus pulposus was dispersed into homogeneous clumps of cells. Subsequently, the cells were transferred to 25 T gas-permeable flasks and cultured in DMEM/F12 medium (BasalMedia, China, L310KJ) supplemented with 15% fetal bovine serum (Sigma-Aldrich, USA; 12,207C) and 1% penicillin–streptomycin (BasalMedia, China, S110JV) at 37°C in a humidified atmosphere with 5% CO_2. After three passages, the cells showed homogenous morphological features, with long spindle-shaped cells constituting almost

Table I. Patient information.

Variable	MDD	SDD	p-value*
Sex			0.558
Female	2	3	
Male	4	3	
Age, yrs			0.079
< 45	4	1	
> 45	2	5	
BMI, kg/m²			0.558
< 24	3	4	
> 24	3	2	
Position	T12-L1	L4-L5	
	L2-L3	L5-S1	
	L1-L2	L4-L5	
	T11-T12	L4-L5	
	C5-C6	L4-L5	
	T12-L1	L5-S1	
Degenerative grades			
I	1		
II	5		
III		1	
IV		3	
V		2	

*Independent-samples *t*-test.
MDD, mildly degenerated intervertebral discs; SDD, severely degenerated intervertebral discs.

the entire population. These third-generation NPCs were used for subsequent experiments.

Cell viability assay

The viability of treated NPCs was assessed using the Cell Counting Kit-8 (CCK8; Dojindo, Japan) according to the manufacturer's instructions. Briefly, NPCs were seeded in a 96-well plate at a density of 5×10^3 cells per well, the next day, 100 μL of the assay solution was added to each well under proof conditions. The plates were placed in an incubator, and optical density was measured on a spectrophotometer after two hours.

RNA isolation, cDNA synthesis, and qRT-PCR

Total RNA was extracted from cultured cells using the SteadyPure Universal RNA Extraction Kit (AG, China, AG21017) according to the manufacturer's instructions. RNA concentration was measured on a Nanodrop spectrophotometer (Thermo Fisher Scientific, USA), and complementary DNA (cDNA) was subsequently synthesized. Quantitative real time polymerase chain reaction (qRT-PCR) was performed using SYBR Green Pro Taq HS Premix III (AG) on a real-time PCR system (Bio-Rad, USA). messenger RNA (mRNA) expression levels were evaluated using the 2-ΔCT method. The primer sequences are as follows, DDIT4: forward primer: GTCTGTGTG GAGCAAGGCAAG, reverse primer: TGTAACCAGGGACCAAGGA AGA.; and GAPDH: forward primer: CTACCCACGGCAAGTTCAA C; reverse primer: CCAGTAGACTCCACGACATA.

Protein extraction and western blotting

Western blotting was used to determine protein levels in NPCs. NPCs were seeded in a six-well plate and subjected to different treatments. The cells were lysed with RIPA buffer (Solarbio, China; R0020) supplemented with protease (Epizyme, USA; GRF101) and phosphatase (Epizyme, GRF102) inhibitors for 15 minutes. The samples were transferred to a centrifugal protein purification empty column (Sanko, Japan, 0.1 ml, C006718) and centrifuged at 10,000 rpm/min and 4°C for one minute to collect the liquid in the lower tube as the total protein. After protein concentration was measured using the bicinchoninic acid assay (BCA) method, the extracted proteins were separated on a 7.5% to 12.5% sodium dodecyl sulphate-polyacrylamide gel and transferred to a PVDF membrane (Millipore, USA). The membrane was blocked with a rapid blocking buffer for 15 minutes and incubated with the following primary antibodies overnight at 4°C: anti-MFN1 (A15471), anti-MFN2 (A13606), anti-OPA1 (A9833), anti-DRP1 (A2586), anti-ASC (A1170), anti-ADAMTS5 (A2836), anti-caspase-1 (A0964), horseradish peroxidase (HRP)-conjugated goat anti-rabbit (AS014; abclonal), anti-aggrecan (13880-1-AP), anti-NLRP3 (27458-1 P), anti-DDIT4 (10638-1 P), anti-MMP13 (18165-1 P; Proteintech), anti-GSDMD (#53120), anti-cleaved-caspase-1 (#40499), anti-collagen II (#33340; SAB), and anti-TXNIP (D5F3E; CST) antibodies. The following day, the membrane was washed three times with tris-buffered saline with 0.1% Tween 20 detergent (TBST) for five minutes each time, and incubated with HRP-conjugated goat anti-rabbit secondary antibody (AS014; abclonal) at room temperature for two hours. Subsequently, the membrane was washed thrice with TBST for five minutes each time, and protein bands were visualized using a Millipore developer. Bands from three independent experiments were analyzed using the ImageJ software (National Institutes of Health, USA) to measure the combined density of each blot. β-actin was used as an internal reference.

Lentiviral transfection

The pLenti-CMV-ddit4-Puro overexpression plasmid and a control plasmid were constructed by PPL (Public Protein/Plasmid Library, China) and transfected into cells as described previously.[30] Briefly, NPCs were seeded in a six-well plate at a density of 5×10^5 cells/per well. After the cells adhered to the wall, they were treated with a viral solution (concentration, 1×10^9 TU/ml) and polybrene (5 μg/ml) for transfection. After 24 hours, the fresh medium was replaced, followed by routine culture. The transfected cells were incubated with specific treatment agents, harvested, and analyzed via western blotting and qRT-PCR.

RNAi

RNAi technology was used to knockdown DDIT4. Three siRNAs targeting DDIT4 were synthesized by Gene Pharma (Shanghai, China). The siRNA sequence are as follows: #1: sense, (5'-3') GCUGCUCAUUGAAGAGUGUTT; antisense,

(5'-3') ACACUCUUCAAUGAGCAGCTT123; #2: sense, (5'-3') GUGCCCACCUUUCAGUUGATT; antisense, (5'-3') UCAACUGAAAGGUGGGCACTT; #3: sense, (5'-3') GGUGUCUCUGCCUGACUUUTT; antisense (5'-3'), AAAGUCAGGCAGAGACACCTT. Transfection was performed using the INTERFERin transfection agent according to the manufacturer's instructions. Briefly, NPCs were seeded in a six-well plate at the density of 5 × 10^5 cells/per well. When the cells reached 50% to 70% confluence, siRNAs, Opti-MEM (ThermoFisher Scientific, USA), and INTERFERin (Polyplus, France) were added to the well plate, and fresh medium was replaced after 24 hours. The silencing efficiency was examined via q-PCR and western blotting after 48 hours.

Immunofluorescence analysis

After the cells were treated, they were fixed with 4% paraformaldehyde for 15 minutes at 4°C, washed three times with TBST, and permeabilized with 0.2% TritonX100 for five minutes. The cells were blocked with 5% goat serum for one hour and incubated with the prepared primary antibody (1:200) overnight at 4°C. The following day, the membrane was washed three times with TBST and incubated with fluorescently labelled secondary antibody (Yeasen, 33,306ES60) at room temperature for two hours in the dark. Thereafter, the cells were stained with 4′ ,6-diamidino-2-phenylindole (DAPI) for five minutes, washed three times with TBST, and imaged using a fluorescence microscope.

JC-1 and ROS staining

Changes in mitochondrial membrane potential and reactive oxygen species (ROS) were observed in myeloid cells using JC-1 and dichloro-dihydro-fluorescein diacetate (DCFH-DA), respectively. NPCs were seeded in a 24-well plate at a density of 1 × 10^5 cells/per well and treated with specific agents. Subsequently, 500 μL of JC-1 solution (1 μL of JC-1 solution per 1 ml of preheated staining buffer) or 500 μL of a pre-prepared staining solution (DCFH-D diluted with serum-free medium (1:1,000)) was added to each well, and the cells were incubated in a 5% CO_2 incubator at 37°C for 30 minutes. The cells were washed once with pre-warmed phosphate-buffered saline (PBS) and observed under a fluorescence microscope and flow cytometry.

Preparation of siDDIT4@G5-P-HA hydrogels and agarose gel electrophoresis

Fifth-generation amino-terminal-containing PAMAM was diluted to a concentration of 4 μM with sterile deionized water, whereas siRNAs were diluted to 2 μM. As described by Chen et al,[31] solutions containing PAMAM and siRNA at the charge ratio (N:P) of 64:1 to 0.2:1 were prepared and shaken sufficiently. The ability of PAMAM to carry siRNAs stably was assessed via agarose gel electrophoresis, and the gel was imaged to determine the appropriate ratio at which siDDIT4 was completely adsorbed by PAMAM. Prepared siDDIT4 and PAMAM solution (siDDIT4@G5-P) was coated with hyaluronic acid (HA). Different solutions of HA monomers and PAMAM were prepared at charge ratios (C:N) ranging from 20:1 to 0.1:1. The stability of HA-coated siDDIT4@G5-P (siDDIT4@G5-P-HA) was evaluated via agarose gel electrophoresis.

Characterization of siDDIT4@G5-P-HA

The zeta potential of siDDIT4@G5-P-HA was measured using a zeta potential analyser (Malvern, UK). The size and morphology of the core particles of siDDIT4@G5-P-HA were observed on a transmission electron microscope (Hitachi HT7700 microscope, 100 kV; Japan).

Analysis of cellular uptake

To assess the uptake of siDDIT4@G5-P-HA by NPCs, the end of siDDIT4 was labelled with cy3. Briefly, NPCs were seeded in 24-well plates at a density of 1 × 10^5. After the cells adhered to the wells, siDDIT4@G5-P-HA solutions with different charge ratios (C: N) were added, and fresh medium was replaced after one day. After three days, the nucleus was stained with DAPI for five minutes, and the cells were washed three times with PBS. Subsequently, fluorescence intensity was observed under a fluorescence microscope.

Silencing efficiency of siDDIT4@G5-P-HA

To assess the silencing efficiency of siDDIT4@G5-P-HA, NPCs were transfected with siDDIT4@G5-P-HA using INTERFERin and cultured routinely. Total protein was extracted after three days, and the silencing efficiency was detected via western blotting.

Animals

The authors of this study followed the ARRIVE guidelines for animal experiments. Disc degeneration was induced in the caudal disc of Sprague-Dawley rats (eight weeks old, weight, 200 g (± 20 g)) via acupuncture as described in a previous study.[29] Briefly, the rats were anaesthetized with isoflurane and fixed in a prone position on an immobilizer. The fifth and sixth caudal discs were located and marked with a permanent marker, and rat tails were disinfected three times with 75% alcohol. A 21-gauge needle was carefully passed vertically through the annulus fibrosus, subsequently inserted into the centre of the disc and eventually passed through the contralateral annulus fibrosus. The needle was controlled to enter at the same depth for each operation, rotated 360°, and held for 30 seconds. Rats in the sham group were anaesthetized, fixed, and sterilized as described above. However, the 21-gauge needle was only inserted into the skin, and no further surgical procedures were performed. Standard postoperative assessments were performed, with behavioural monitoring every alternative day for six weeks (after the puncture); no signs of pain or distress were observed upon monitoring. After the models were established, the rats were randomly divided into four groups (n = 6) as follows: control, cy3-siDDIT4@G5-P-HA, cy3-siDDIT4, and acupuncture groups. Rats in the control group did not receive any treatment, rats in the acupuncture group received acupuncture without any subsequent treatment, and rats in the two experimental groups received 50 μL solution containing 100 nM siDDIT4 of cy3-siDDIT4@G5-P-HA or cy3-siDDIT4 after IVDD was induced via acupuncture. Since the model was established on day 1 after surgery, the fluorescence intensity of the rat tail intervertebral disc was observed on an IVIS. Imaging was performed every seven days postoperatively to monitor the fluorescence intensity. Subsequent experiments were performed after five weeks.

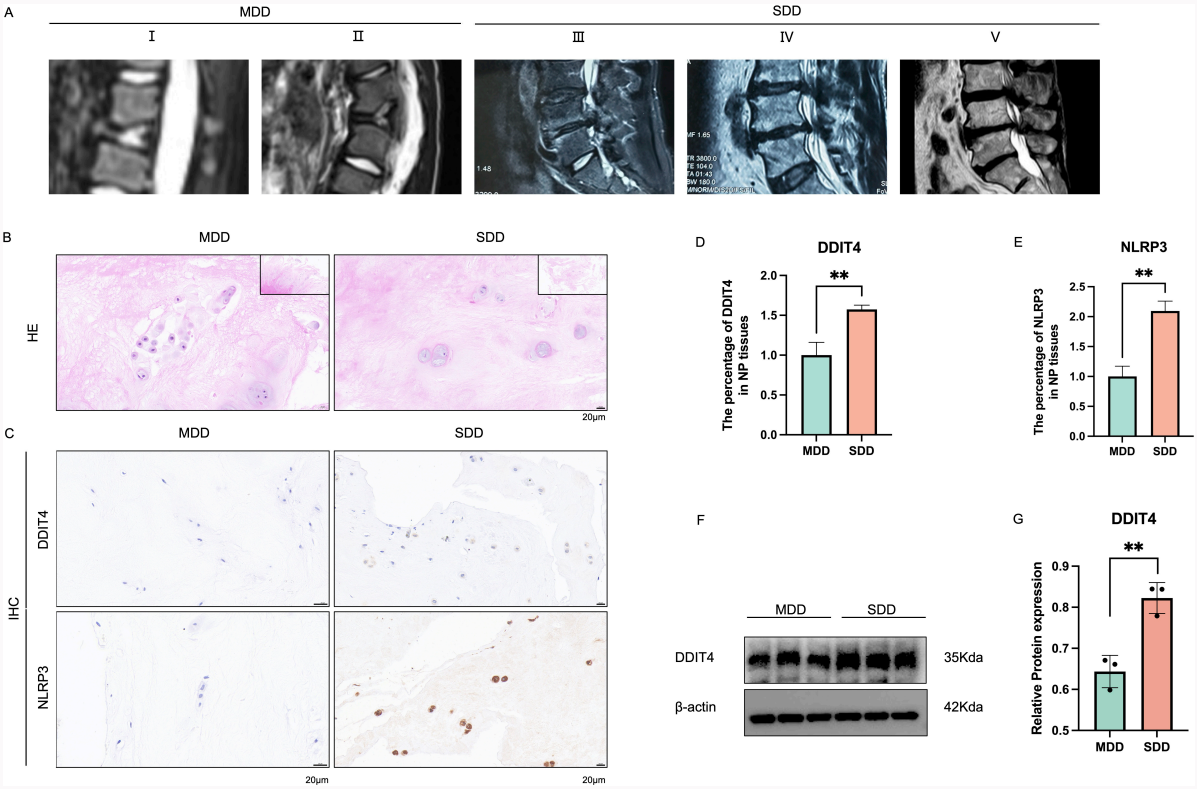

Fig. 1

DDIT4 expression is upregulated in the intervertebral discs of patients with intervertebral disc degeneration (IVDD) and rat models of acupuncture-induced IVDD. a) Representative MRI images of mildly degenerated discs (MDD, Pfirrmann grades I to II) and severely degenerated discs (SDD, Pfirrmann grades III to V) in human patients with IVDD. b) Haematoxylin and eosin (H&E) staining in the MDD and SDD groups (n = 6); scale bars, 20 μm. c) to e) Immunohistochemical (IHC) staining of DDIT4 and NLRP3 and quantitative analysis of positively stained cells in the tissues of the MDD and SDD groups (n = 6); scale bars, 20μm. f) and g) Western blotting and quantitative analysis of DDIT4 in the MDD and SDD groups. Scale bars in overall view: 200 μm; scale bars in local view: 20 μm. Data are expressed as the mean and standard deviation (*p < 0.05; **p < 0.01).

Statistical analysis

All data are expressed as the mean and standard deviation (SD) of at least three independent experiments. One-way analysis of variance (ANOVA) was used to compare the data of three or more groups, whereas theindependent-samples *t*-test was used to compare the data of two groups. The GraphPad Prism 9.0 software (GraphPad, USA) was used for statistical analysis. A p-value of < 0.05 indicated statistical significance.

Results

DDIT4 expression was upregulated in human degenerative discs and rat models of disc degeneration

Haematoxylin and eosin (H&E) staining showed the presence of less abundant, clustered NPCs in SDD, and immunohistochemical (IHC) staining showed that the expression of DDIT4 and NLRP3 was higher in SDD than in MDD (Figures 1b to 1e). Subsequently, western blotting revealed that the expression of DDIT4 was low in MDDs but high in SDD (Figures 1F to G). Furthermore, changes in the expression of DDIT4 and NLRP3 were verified in rats (n = 6), the detailed animal model method for which is shown in Supplementary Figure a. H&E staining showed that the NP contained abundant ECM and was well differentiated from the AF in the sham group. However, in degenerated discs, the abundance of resident cells was low and the ECM was degraded (Supplementary Figure a). In vivo IHC analysis showed significantly higher expression of DDIT4 and NLRP3 in the degenerated group than in the sham group (Supplementary Figure a).

Oxidative stress triggered DDIT4 upregulation and pyroptosis in NP cells

We isolated primary rat NPCs and treated them with different concentrations of hydrogen peroxide (H_2O_2, 0 to 1,000 μM) for 24 hours to establish an in vitro model of IVDD, following the methods of previous researchers (Figure 2a).[32] The concentrations of 200 μM and 400 μM, which had a minimal but significant effect on the proliferation of NPCs, were considered optimal for use in subsequent experiments. qRT-PCR revealed that the mRNA expression of DDIT4 was upregulated in NPCs treated with H_2O_2 (Figure 2b). Immunofluorescence analysis revealed that the fluorescence intensity of DDIT4 was enhanced in NPCs treated with H_2O_2 (Figure 2c). Western blotting showed that increased expression of DDIT4 in H_2O_2-treated NPC in a concentration-dependent manner was accompanied by a decrease in two important ECM-associated proteins,[33] COL2A1 and ACAN, and an increase in MMP13 and ADAMTS5, which are involved in the degradation of the ECM (Figures 2d to 2i).[34] To explore pyroptosis in NPCs under oxidative stress, the expression of NLRP3, ASC, cleaved GSDMD, cleaved CASP1, and IL-1β increased in a concentration-dependent manner in H_2O_2-treated NPCs (Supplementary Figure b). Subsequently, transmission electron microscopy (TEM) was used to observe the ultrastructure of

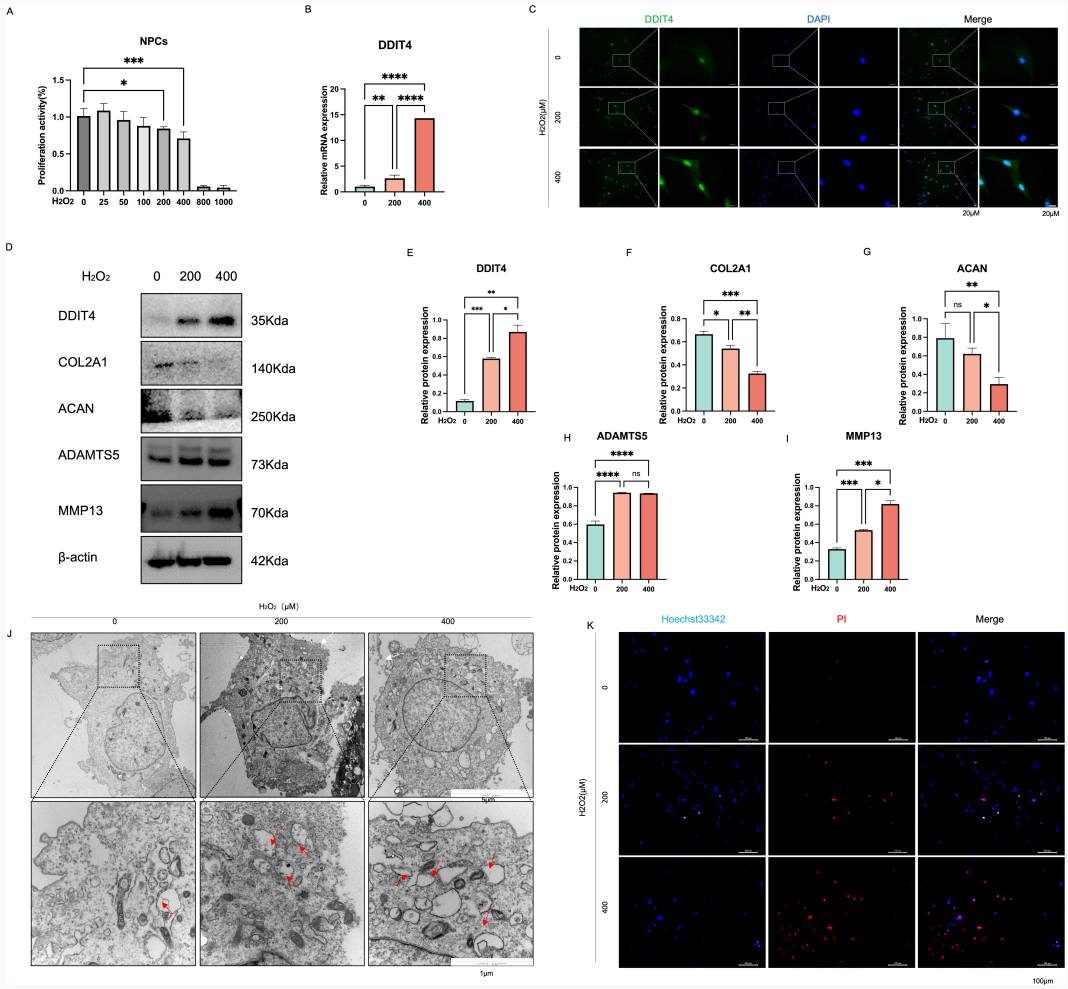

Fig. 2

Oxidative stress triggers DDIT4 upregulation and pyroptosis in nucleus pulposus cells (NPCs). a) Quantitative analysis of the viability of rat NPCs cultured with different concentrations (0 to 1,000 μM) of hydrogen peroxide for 24 hours. b) Select rat NPCs were incubated with different concentrations of hydrogen peroxide (0, 200, and 400 μM) for 24 hours, qRT-PCR analysis of DDIT4 mRNA expression levels in rat NPCs exposed to 0, 200, and 400 μM hydrogen peroxide. Error bars are the mean and standard deviation (n = 3); **p < 0.01, ***p < 0.001.and ****p < 0.0001, independent-samples *t*-test. c) Immunofluorescence analysis of DDIT4 in hydrogen peroxide-treated NPCs and control NPCs; scale bars, 20 μm. d) to i) Representative western blotting images and quantitative analysis of DDIT4, COL2A1, ACAN, ADAMTS5, and matrix metalloproteinase 13 (MMP13) in hydrogen peroxide-treated NPCs and control NPCs. j) Transmission electron microscope images of hydrogen peroxide-treated NPCs, such as cytoplasmic oedema, swelling of cell membrane, karyopyknosis, and organelle cavitation, white arrows show swelling of cell membrane; red arrows show organelle cavitation, Scale bars in overall view: 5 μm; scale bars in local view: 1 μm. k) Representative fluorescence images of Hoechst 33342/PI-stained hydrogen peroxide-treated NPCs; scale bars, 20 μm. Data are expressed as the mean and standard deviation of at least three independent experiments. Two-way analysis of variance was used for statistical analysis (*p < 0.05; **p < 0.01; ***p < 0.001; ****p < 0.0001).

NPCs. H_2O_2-treated NPCs had large vacuoles and a perforated and ruptured cell membrane, which are the characteristics of pyroptosis induced by cleaved GSDMD (Figure 2j). Finally, cell viability was assessed via Hoechst and propidium iodide (PI) staining, and the results showed that cell death was significantly increased after H_2O_2 treatment (Figure 2k).

Upregulation of DDIT4 aggravated the pyroptosis of NPCs under oxidative stress

To investigate whether DDIT4 upregulation promoted the pyroptosis and dysfunction of H_2O_2-treated NPCs, the cells were transfected with pLenti-CMV-ddit4-Puro lentivirus to overexpress DDIT4. Immunofluorescence (IF) analysis showed that the expression of DDIT4 was significantly higher in the overexpression group than in the control group and the empty vector group (Figure 3a). Western blotting revealed that DDIT4 overexpression significantly decreased the protein expression of COL2A1 and ACAN, and significantly increased the protein expression of MMP13 and ADAMTS5 (Figures 3B to G). Furthermore, quantitative analysis of western blotting and enzyme-linked immunosorbent assay (ELISA) revealed that DDIT4 overexpression significantly increased the expression of NLRP3, ASC, cleaved GSDMD, cleaved CASP1, and IL-1β (Supplementary Figure c). Additionally, the rupture of the cell membrane and formation of intracellular vacuoles were more pronounced in the overexpression group than in the control group and empty vector group (Figure 3h). Hoechst and PI staining showed that the rate of cell death was significantly higher in the overexpression group (Figure 3i). At the same time, we applied siRNA to knock down DDIT4. Three sets of siRNAs (numbered 1 to 3) were used to knock down DDIT4; the third set of siRNAs, which had the best silencing efficiency, was selected for subsequent experiments and observed the

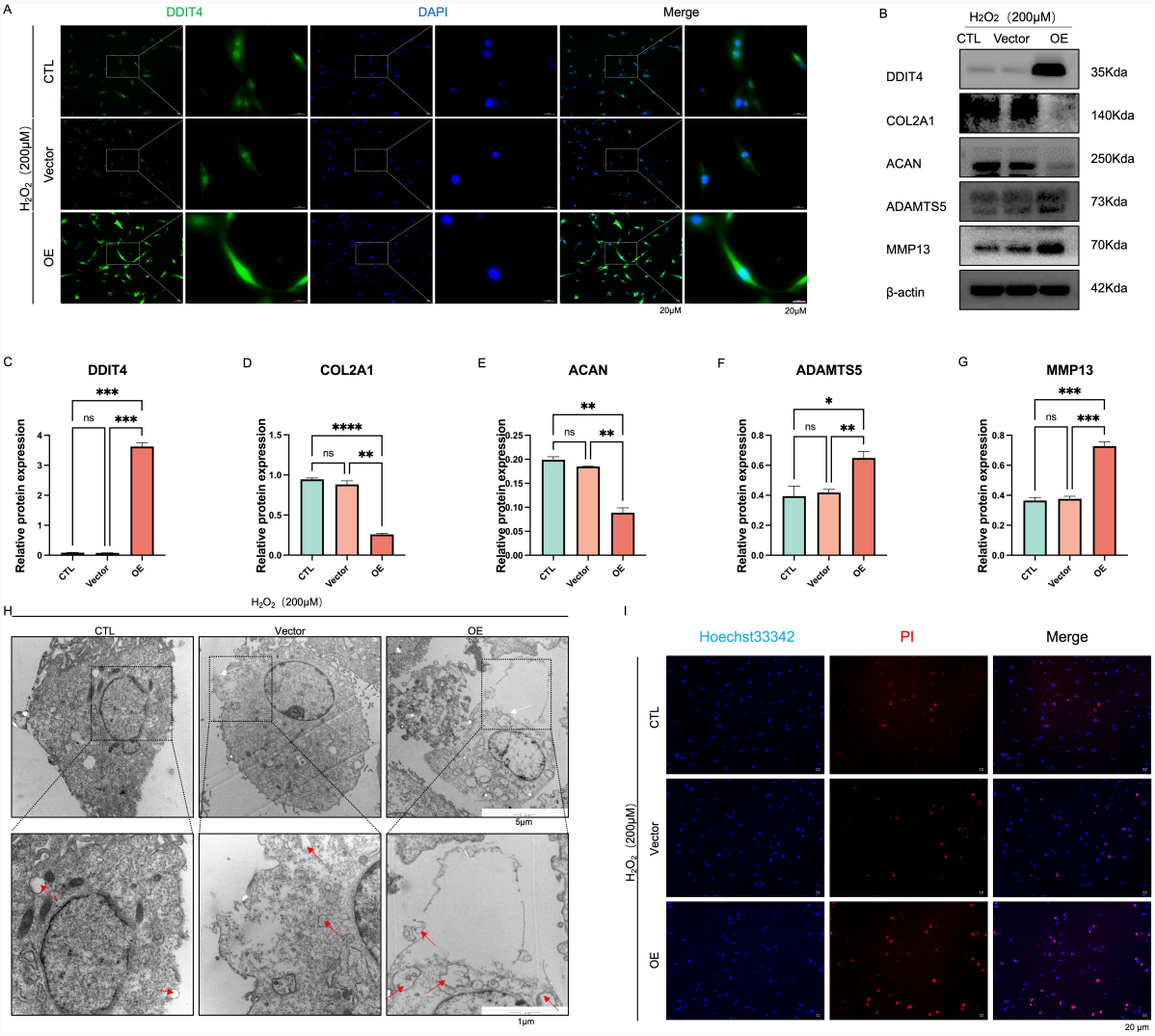

Fig. 3

Upregulation of DDIT4 aggravates pyroptosis of nucleus pulposus cells (NPCs) under oxidative stress. DDIT4 was overexpressed in NPCs, and NPCs were treated with 200 μM hydrogen peroxide for 24 hours. a) Immunofluorescence analysis of DDIT4 after hydrogen peroxide treatment in the control, vector, and overexpression groups; scale bars, 20 μm. b) to g) Representative images of western blotting and quantitative analysis of DDIT4, COL2A1, ACAN, ADAMTS5, and matrix metalloproteinase 13 (MMP13) in the control, vector, and overexpression groups after hydrogen peroxide treatment. h) Transmission electron microscope images of NPCs treated with hydrogen peroxide in the control, vector, and overexpression groups, such as cytoplasmic oedema, swelling of cell membrane, karyopyknosis, and organelle cavitation; white arrows show swelling of cell membran, while red arrows show organelle cavitation. Scale bars in overall view: 5 μm; scale bars in local view: 1 μm. i) Representative fluorescence images of Hoechst 33342/PI staining of NPCs treated with hydrogen peroxide in the control, vector, and overexpression groups. Scale bars, 20 μm. Data are expressed as the mean and standard deviation of at least three independent experiments. Two-way analysis of variance was used for statistical analysis (ns, no statistical significance; *p < 0.05; **p < 0.01; ***p < 0.001; ****p < 0.0001).

opposite result to overexpression (Supplementary Figures d to j).

DDIT4 impaired the mitochondrial function of NPCs and promoted ROS generation

Given that DDIT4 promotes the pyroptosis of NPCs, we identified pathways involved in this process. Previous studies have reported that endogenous DDIT4 localises to mitochondria.[35,36] The mitochondria-selective fluorescent probe MitoTracker and IF of DDIT4 were used to examine the location of DDIT4 in NPCs. The two fluorescence intensities were diametrically opposed; nevertheless, they can be merged (Figures 4a to 4c). The function of mitochondria is closely related to their morphology. To examine the effects of DDIT4 on mitochondrial function, we evaluated the expression of proteins related to mitochondrial morphology and function, including dynamin-related peptide 1 (Drp1), optic atrophy 1 (OPA1), mitofusin 1/2 (MFN1/2), and AMP-activated protein kinase (AMPK). Overexpression of DDIT4 increased the expression of DRP1, MFN1, and MFN2, and decreased the expression of p-AMPK. However, it did not affect the expression of OPA1. In contrast, knocking down DDIT4 showed the opposite result (Figures 4d to 4i). To further examine the effects of DDIT4 on mitochondrial function, JC-1 staining was used to detect mitochondrial membrane potential. The red fluorescence intensity was lower and the green fluorescence intensity was higher in the overexpression group than in the control group, whereas contradictory effects were observed in the knockdown group (Supplementary Figure k). The results of flowcytometry were similar to

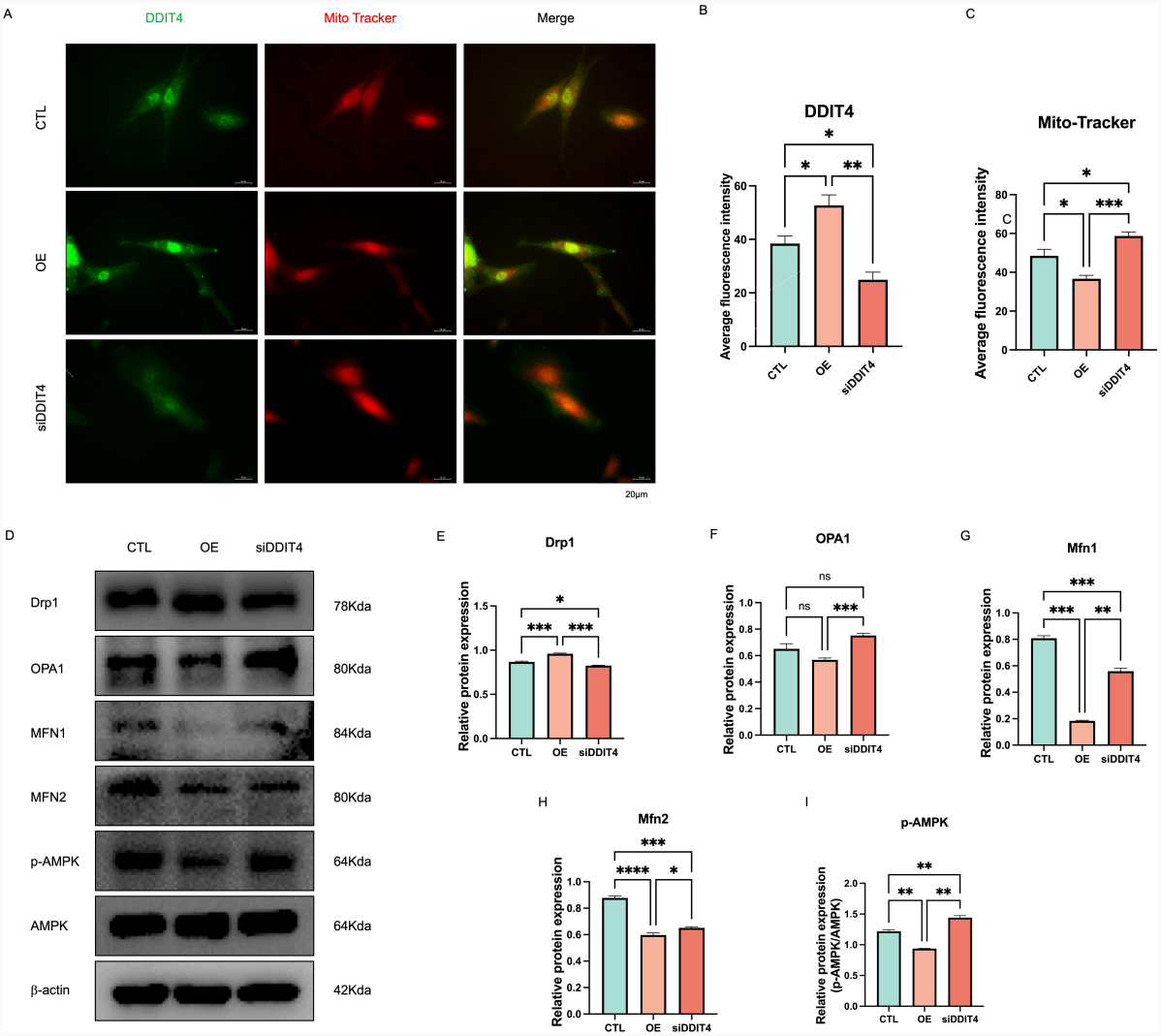

Fig. 4
DNA-damage-inducible transcript 4 (DDIT4) impairs mitochondrial function and promotes reactive oxygen species (ROS) generation nucleus pulposus cells (NPCs) in the control, overexpression, and knockdown groups were cultured for 24hours. a)Representative fluorescence images of DDIT4 (green) and MitoTracker (red) double staining for different degrees of aggregation; scale bars: 20μm. b) Quantitative analysis of DDIT4 fluorescence intensity. c) Quantitative analysis of MitoTracker fluorescence intensity. d) to i) Representative images of western blotting of DRP1, OPA1, MFN1, MFN2, and p-AMPK in the control, overexpression, and knockdown groups, with β-actin used as a control. Data are expressed as the mean and standard deviation of at least three independent experiments. Two-way analysis of variance was used for statistical analysis (ns, no statistical significance; *p < 0.05; **p < 0.01; ***p < 0.001; ****p < 0.0001).

those of JC-1 staining (Supplementary Figure k). Intracellular ROS production was assessed using the DCFH-DA probe. As shown in (Supplementary Figure k), the green fluorescence intensity was stronger in the overexpression group but weaker in the knockdown group. Flow cytometry revealed similar results (Supplementary Figure k).

DDIT4 regulates NP pyroptosis through the ROS-TXNIP-NLRP3 axis

To examine the relationship between DDIT4 and pyroptosis, we used the STRING database to examine the interaction of DDIT4 with other proteins.[37] A total of 16 proteins were found to interact with DDIT4 (Figure 5a). Overall, 436 pyroptosis-related genes were identified using Genecards,[38] with five genes being common between the two database searches (Figure 5b). Subsequently, KOBAS was used for enrichment analysis.[39] It can be seen that the enrichment is mainly on the NOD-like receptor signalling pathway and on the pathogenesis of IVDD (Figure 5C–D). As shown in Figure 5a, thioredoxin-interacting protein (TXNIP) acts as a bridge between DDIT4 and NLRP3. Because of this, we used N-acetylcysteine (NAC) to scavenge ROS in NPCs. DCFH-DA was used to examine the levels of ROS in NPCs. The fluorescence intensity was significantly lower in the NAC group than in the H_2O_2 group (Figures 5E and 5G); flowcytometry revealed similar results (Figure 5f). Western blotting validated that the expression of DDIT4 and TXNIP was upregulated after H_2O_2 treatment, but downregulated after NAC treatment (Figure 5H–J). Furthermore, the relationship among DDIT4, TXNIP, ROS, and pyroptosis was examined. Western blotting revealed that the expression of NLRP3, ASC, cleaved GSDMD, and cleaved CASP1 was upregulated after hydrogen peroxide treatment but was significantly downregulated after NAC treatment (Supplementary Figure l). The results of ELISA demonstrated the same trend for IL-1β expression (Supplementary Figure l).

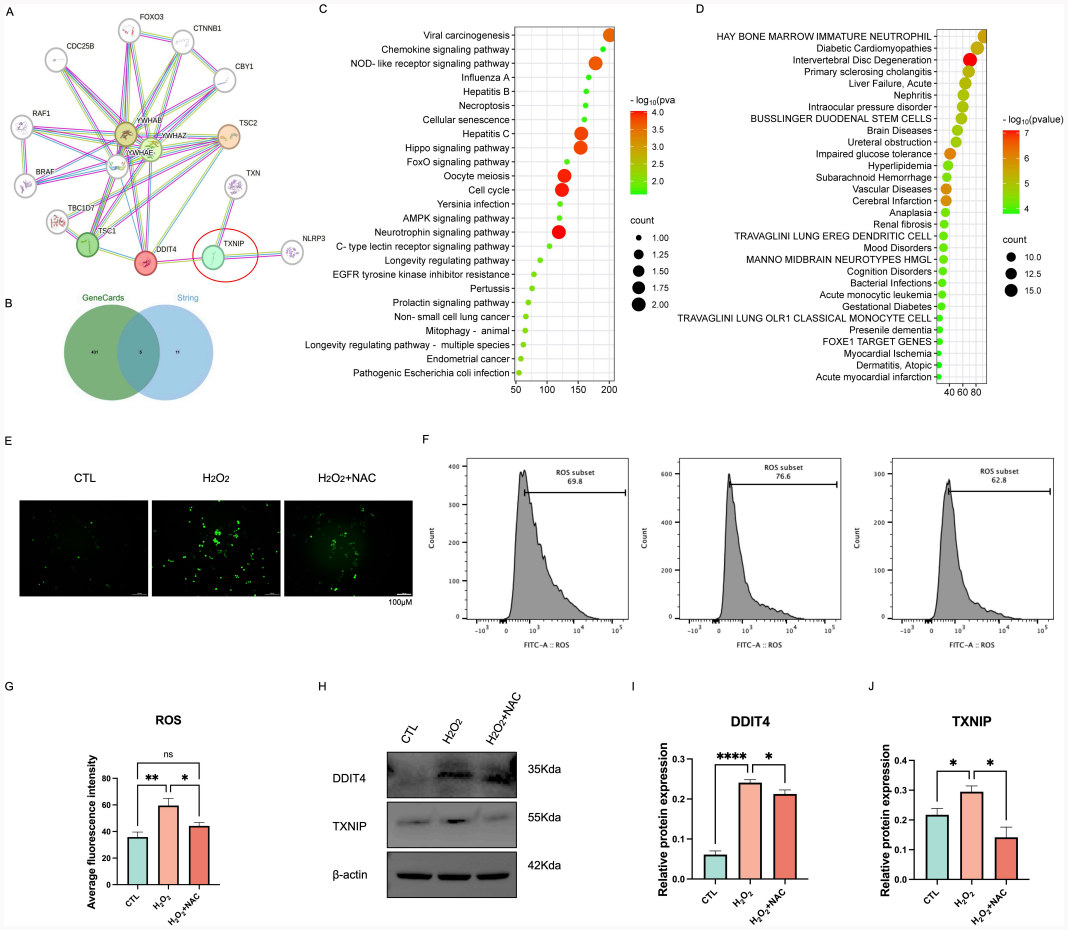

Fig. 5

DNA-damage-inducible transcript 4 (DDIT4) mediated pyroptosis of nucleus pulposus cells (NPCs) through the ROS-NLRP3-CASP1 axis. a) Protein-protein interaction network of DDIT4 in the STRING database. b) Venn diagram of genes associated with DDIT4 in the STRING database and genes associated with disc degeneration in the Genecards database. c) Bubble chart of Kyoto Encyclopedia of Genes and Genomes (KEGG) disease analysis. d) Bubble chart of KEGG pathway analysis. e) The dichloro-dihydro-fluorescein diacetate (DCFH-DA) probe was used to detect ROS in NPCs in the control, hydrogen peroxide treatment, and N-acetylcysteine (NAC) treatment groups. Green fluorescence represents intracellular ROS levels; scale bars: 20 μm. g) Quantitative analysis of ROS staining in the control, hydrogen peroxide treatment, and NAC treatment groups. f) Flow cytometry was performed using the DCFH-DA probe to detect ROS in the control, hydrogen peroxide treatment, and NAC treatment groups. h) to j) Representative images of western blotting and quantitative analysis of DDIT4 and thioredoxin-interacting protein (TXNIP) in NPCs in the control, hydrogen peroxide treatment, and NAC treatment groups. Data are expressed as the mean and standard deviation of at least three independent experiments. Independent-samples *t*-test and two-way analysis of variance were used for statistical analysis (ns, no statistical significance; *p < 0.05; **p < 0.01; ***p < 0.001).

Design and synthesis of siDDIT4-delivering hydrogels

The aforementioned results indicate that knockdown of DDIT4 represents a novel strategy for inhibiting oxidative stress-induced pyroptosis of NPCs. Therefore, in this study, we designed a novel composite material capable of delivering siDDIT4 for treating IVDD. Among siRNA carriers, fifth-generation PAMAM-NH_2 (Figure 6a) has branched chains that can be extended and expanded to form a molecular skeleton and derive a molecular 'gap', and has terminal positively charged amino groups.[40,41] Additionally, we used hyaluronic acid (HA) with excellent biocompatibility for terminal modification (Figure 6b). Agarose gel electrophoresis was performed to determine the optimal charge ratio (N/P) of PAMAM and siDDIT4. As shown in Figure 7c, siDDIT4 was completely adsorbed on PAMAM when the N/P ratio was > 20. Given that the cytotoxicity of PAMAM is mainly attributed to its strong polarity, we selected the N/P ratio of 20 for subsequent experiments. HA was used to encapsulate siDDIT4@G5-P, and agarose gel electrophoresis was performed to determine the optimal charge ratio of HA-coated PAMAM (HA monomer and PAMAM charge ratio, C/N) (Figure 6d). At a C/N ratio of < 1.25, HA could adequately coat siDDIT4@G5-P, forming a triplex composite hydrogel (siDDIT4@G5-P-HA). Furthermore, the zeta potential of siDDIT4@G5-P-HA hydrogel was evaluated, the mean zeta potential of naked G5-PAMAM-NH_2 was +34.33333 mV (SD 1.0873), whereas that of siDDIT4@G5-P-HA hydrogel was+ 7.77 mV (SD 0.197989899) (Figure 6E–F). Subsequently, TEM was used to assess the morphology and size of siDDIT4@G5-P-HA hydrogel. TEM images showed that siDDIT4@G5-P-HA hydrogel was spherical with a diameter of approximately 100 to 200 nm (Figure 6G–H).

siDDIT4@G5-P-HA hydrogel was internalized by NPCs and effectively silenced DDIT4

Rat NPCs were treated with siDDIT4@G5-P-HA hydrogel or transfection reagent containing 100 nM siDDIT4, and their viability was assessed via cell counting kit-8 (CCK8) assay. Cell viability, with peaks at 0.6 and 1.25, showed

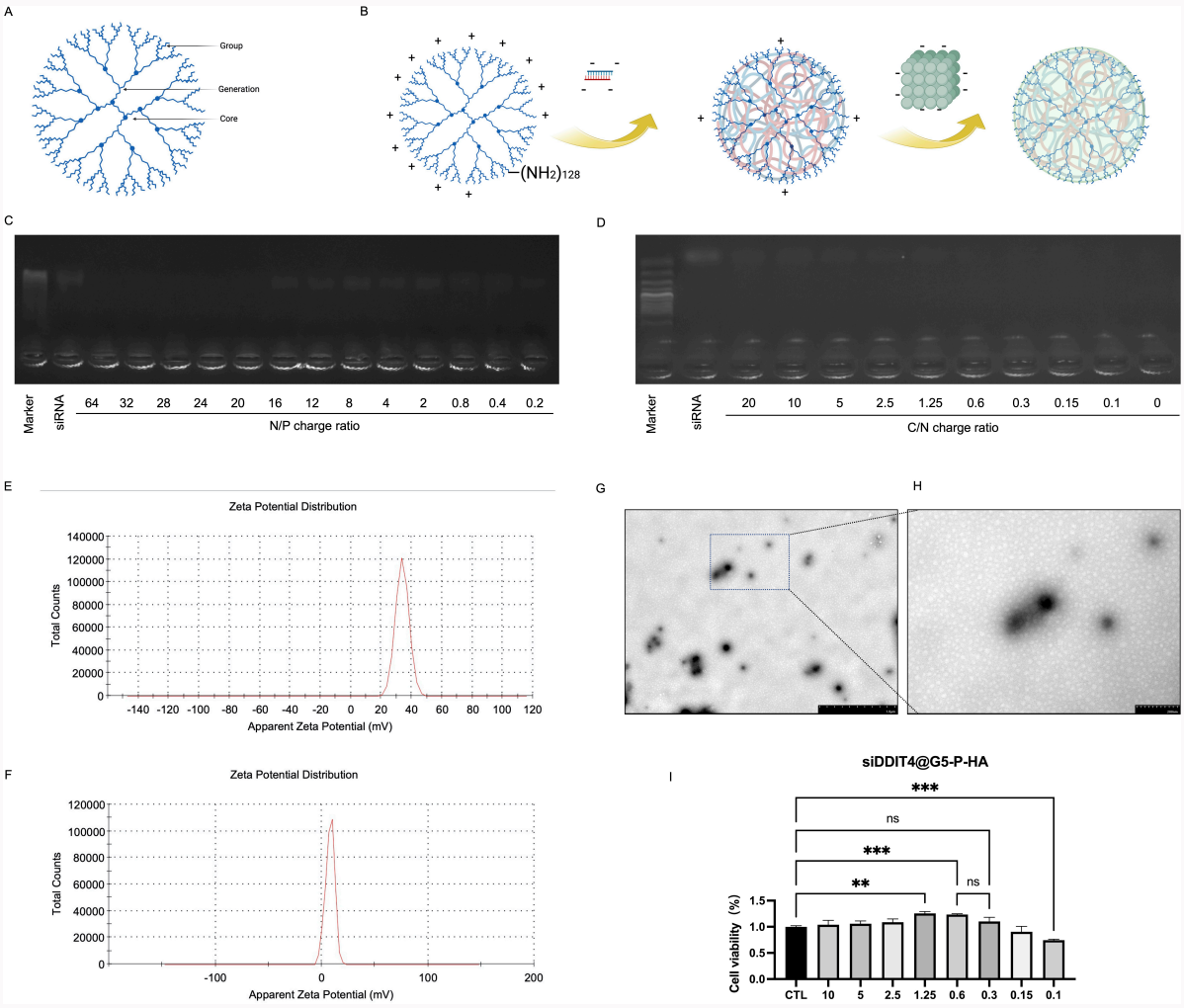

Fig. 6

Preparation of siDDIT4@G5-P-HA hydrogels and assessment of its cellular uptake and silencing efficiency. a) Schematic diagram of the molecular structure of PAMAM. b) Schematic diagram demonstrating the preparation of siDDIT4@G5-P-HA hydrogels (van der Waals forces). c) Agarose gel electrophoresis of siDDIT4@G5-P composed of PAMAM and small interfering RNAs (siRNAs) at different charge ratios (N/P ratios). d) Agarose gel electrophoresis of hyaluronic acid-coated siDDIT4@G5-P at the N/P ratio of 20. e) and f) Zeta potential of pristine PAMAM and siDDIT4@G5-P-HA hydrogels. g) and h) Transmission electron microscopy (TEM) images of siDDIT4@G5-P-HA hydrogels with different degrees of polymerization; scale bars in overall view: 1 μm; scale bars in local view: 200 nm. i) Quantitative analysis of cell viability after treatment of NPCs with siDDIT4@G5-P-HA hydrogels. Data are expressed as the mean and standard deviation of at least three independent experiments. Two-way analysis of variance and independent-samples *t*-test were used for statistical analysis (ns, no statistical significance; *p < 0.05; **p < 0.01; ***p < 0.001).

a tendency to increase and then decrease with C/N ratio. (Figure 6i). Furthermore, after rat NPCs were transfected with cy3-siDDIT4@Polyplus and cy3-siDDIT4@G5-P-HA, the uptake of siRNAs in vitro was assessed via fluorescence imaging. As shown in (Supplementary Figure m), at C/N ratios ranging from 0.3 to 1.25, the fluorescence intensity remained consistent with that of the PolyPlus. To verify that the hydrogel can maintain the biological activity of siRNAs during release, we detected the protein expression of DDIT4 via western blotting. The protein expression of DDIT4 significantly decreased at C/N ratios of < 1.25. In particular, when the C/N ratio was < 0.6, the silencing efficiency of PAMAM was comparable to the transfection efficiency of Polyplus (Supplementary Figure m). Therefore, a C/N ratio of 0.6 was used for subsequent preparation of hydrogels and for subsequent in vivo experiments.

Sustained therapeutic effects of siDDIT4@G5-P-HA in rat models of acupuncture-induced IVDD

The therapeutic effects of siDDIT4@G5-P-HA hydrogel in vivo were evaluated using rat models of acupuncture-induced IVDD. The detailed experimental procedure is shown in Figure 7a. The rats were divided into four groups (n = 6): cy3-siDDIT4@G5-P-HA, cy3-siDDIT4, acupuncture, and control. The rats were imaged on in vivo imaging system (IVIS) on the day of surgery and once a week until five weeks thereafter. Fluorescence in the cy3-siDDIT4 group had completely disappeared after 21 days of treatment, whereas fluorescence was observed in the cy3-siDDIT4@G5-P-HA group after 35 days of treatment (Figure 7B–C). In addition, the body weight of rats in the four groups was regularly monitored (Figure 7d). T2-weighted MRI was used to determine the water content in rat intervertebral discs. The cy3-siDDIT4@G5-P-HA and control groups demonstrated stronger signals than the cy3-siDDIT4 group, whereas the acupuncture group demonstrated a weak

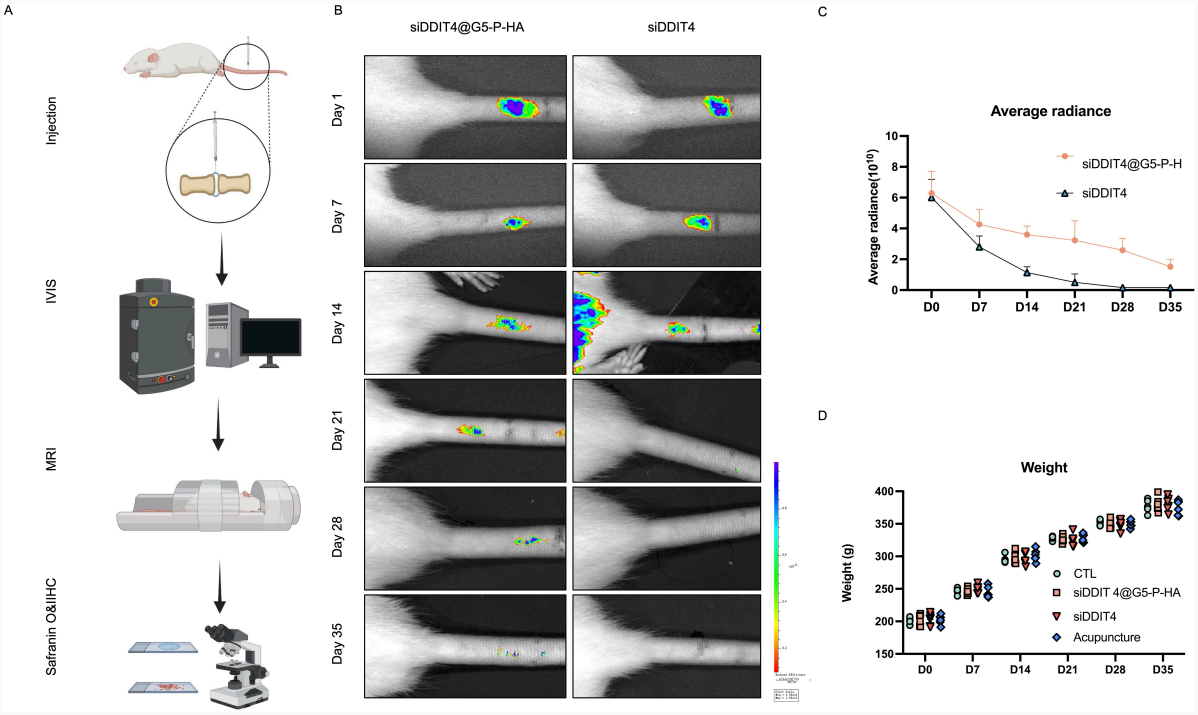

Fig. 7
siDDIT4@G5-P-HA delays the progression of intervertebral disc degeneration (IVDD) in rat models of acupuncture-induced IVDD. a) Overview of animal experimental procedures. b) Representative images of in vivo imaging of rats from day 0 to day 35 after cy3-siDDIT4@G5-P-HA and cy3-siDDIT4 injection (n = 6). c) Quantification of cy3-siDDIT4 using in vivo imaging system (IVIS). d) Body weight of rats in the control, cy3-siDDIT4@G5-P-HA, cy3-siDDIT4, and acupuncture groups (n = 6).

signal (Supplementary Figure n). Subsequently, T1-weighted MRI was used to evaluate the disc height index (DHI) of rats in the four groups.[42] The DHI value of the cy3-siDDIT4@G5-P-HA group was similar to that of the control group, higher than that of the cy3-siDDIT4 group and significantly higher than that of the acupuncture group (Supplementary Figure n). To assess the continuous silencing of DDIT4 by the hydrogel, rat disc tissue was stained with Safranin O fast green and IHC. The control group was rich in ECM, and low expression of DDIT4 and NLRP3. The cy3-siDDIT4@G5-P-HA and cy3-siDDIT4 groups had moderate ECM. The cy3-siDDIT4@G5-P-HA group exhibited higher abundance of ECM, clearer boundary between the nucleus pulposus and annulus fibrosus, and lower expression of DDIT4 and NLRP3 compared to the cy3-siDDIT4 group. Finally, the nucleus pulposus shrank and collapsed, causing a faded boundary between the NP and AF in the acupuncture group. Additionally, the expression levels of DDIT4 and NLRP3 were the highest among all four groups (Supplementary Figure n).

Discussion

In this study, DDIT4 was identified as an important factor contributing to the development of IVDD. The expression of DDIT4 was upregulated under H_2O_2-induced mitochondrial damage, and the interaction of DDIT4 with TXNIP activated the classic pyroptosis pathway. Furthermore, we developed siDDIT4@G5-P-HA hydrogel that delivered and released siDDIT4 in a controlled and continuous manner to inhibit the pyroptosis of NPCs. In vivo experiments demonstrated that only one in situ injection of siDDIT4@G5-P-HA inhibited the pyroptosis of NPCs and the degradation of ECM, thereby attenuating the progression of IVDD in rats. Altogether, this study proposed a new siRNA-based strategy for the treatment of IVDD.

Previous studies have reported that DDIT4 is identified as one of the causes of IVDD and is highly expressed in severely degenerated intervertebral disc tissues.[35,43] A study by Yin et al[35] demonstrated that DDIT4 is involved in the pathological process of IVDD. DDIT4 forms a complex with TXNIP to accelerate the apoptosis of NPCs through the mitochondrial pathway induced by hydrogen peroxide. The aforementioned study suggests that DDIT4 can promote ROS production; therefore, we speculated that DDIT4 is sensitive to oxidative stress. Mitochondria, the energy production unit of the cell, play an important role in regulating cell apoptosis and necrosis, which are associated with irreversible changes in mitochondrial permeability.[44,45] NLRP3 and the inflammasome adapter protein PYD and CARD domains (PYCARD, ASC) re-localize to the mitochondria-associated endoplasmic reticulum after the mitochondrial outer membrane permeability is altered, a process that relies on mitochondrial ROS.[46] Furthermore, optimal NLRP3 inflammasome signalling appears to be involved in the interaction between NLRP3 and TXNIP, a nuclear protein that re-localizes to mitochondria during oxidative stress.[47] Therefore, mitochondrial dysfunction may be closely related to the activation of the NLRP3 inflammasome. We speculated that DDIT4 is located in mitochondria. DDIT4 regulates mitochondrial membrane permeability and ROS, and interacts with TXNIP to activate inflammasomes, thereby activating NP pyroptosis, stimulating IL-β release and eventually leading to the occurrence and progression of IVDD. We validated the co-localization of DDIT4 and mitochondrial

MitoTracker via IF analysis and found that it was negatively associated with the mitochondrial membrane potential. These results are consistent with those of previous studies.

SiRNAs can be used to specifically silence a certain gene ("silence the gene, silence the disease").[48] At present, the main obstacle to using siRNA-based therapeutics in clinical practice is the lack of an effective delivery system to protect siRNAs from nuclease degradation. Donald A. Tomalia first reported PAMAM dendrimers in 1985.[49] PAMAM is one of the most used dendrimers in drug and siRNA delivery systems. It serves as a delivery vehicle in the following three ways: generation of a void (via molecular entrapment), branch point (via hydrogen bonding), and external surface group passage (via charge-charge interactions).[50] In a study, G4-PAMAM-NH_2 was used to deliver the acidic drug indometacin and demonstrated good solubility. However, when G4-PAMAM-COOH was used to deliver indometacin, the effect was poor.[51] We hypothesized that the terminal of PAMAM is critical for siRNA delivery. Another study has compared the effects of second-, third-, and fourth-generation PAMAM on the efficiency of siRNAs in silencing the TEL protein. The silencing efficiency of fourth-generation PAMAM was better than that of second- and third-generation PAMAM. Altogether, the three generations of PAMAM showed good silencing efficiency, and no significant differences were observed in their cytotoxicity.[52] Fluorination can improve the efficiency of 4-7-generation PAMAM in delivering DNA and siRNA; however, fifth-generation PAMAM is considered the optimal polymer for gene delivery.[53] In this study, we selected the terminal amino group of fifth-generation PAMAM as the carrier. The terminal of PAMAM is often modified to improve its decomposition efficiency after transfection, confer PAMAM with targeting ability, and reduce its cytotoxicity. Given that HA can bind to CD44,[54] HA-coated PAMAM has been designed to deliver chemotherapeutic drugs or siRNAs to improve their targeting ability.[55,56] HA is not only related to tumour metastasis but also an important component of normal human tissues. It is widely distributed in the intercellular matrix, vitreous body, and joint fluid.[57] In addition, it forms the backbone of type 2 collagen and glycosaminoglycan, which are important extracellular matrix-related proteins, in the intervertebral disc.[1] Given that NPCs are CD44-positive,[58] siRNA-carrying PAMAM may readily anchor the cells, whereas HA may facilitate the controlled release of siRNAs. Therefore, in this study, we selected fifth-generation PAMAM as the delivery vehicle of siDDIT4 and used HA to coat PAMAM.

This study has several strengths. We demonstrated that DDIT4 is one of the factors that promote the development of IVDD and designed in situ injectable siDDIT4@G5-P-HA hydrogels using RNAi technology, providing a novel strategy for the treatment of IVDD. However, the limitations of this study should also be acknowledged. First, the sample size was small (six patients). Second, we used an IVIS to observe the duration of fluorescence in rat intervertebral discs and did not design specific in vitro experiments to validate the controlled release of siRNAs from siDDIT4@G5-P-HA hydrogels. Finally, a good siRNA carrier should not only serve as a delivery vehicle, but also have the ability to penetrate cells without getting accumulated. Excessive accumulation of siRNA carriers may affect cell viability or state in the long term; therefore, an ideal carrier should be biodegradable. Degradable dendrimers with gallic acid as the core, triethylene glycol as the branch chain, and PEG modification at the end have been designed in a previous study.[59] We will design more appropriate experiments in future studies to address the aforementioned limitations and develop novel therapeutic strategies for IVDD.

DDIT4 plays a deleterious but important role in human IVDD, verified in rat models of acupuncture-induced IVDD. Oxidative stress induces mitochondrial damage and enhances the localization of DDIT4 to mitochondria. In addition, ROS induction activates the ROS-TXNIP-NLRP31 axis, thereby inducing NP pyroptosis and promoting the development of IVDD. The in situ injectable hydrogel designed in this study consisted of siDDIT4, PAMAM and HA, which were integrated via van der Waals forces. This hydrogel efficiently delivered siDDIT4 and subsequently silenced DDIT4 expression in NPCs. In situ injection of this composite hydrogel into rat intervertebral discs attenuated NP pyroptosis and alleviated IVDD by prolonging the silencing of DDIT4.

Supplementary material

Additional figures.

References

1. **Kritschil R**, **Scott M**, **Sowa G**, **Vo N**. Role of autophagy in intervertebral disc degeneration. *J Cell Physiol*. 2022;237(2):1266–1284.
2. **Yurube T**, **Han I**, **Sakai D**. Concepts of regeneration for spinal diseases in 2023. *Int J Mol Sci*. 2023;24(22):16335.
3. **Yoo H**, **Yoo R-E**, **Choi SH**, **et al**. Deep learning-based reconstruction for acceleration of lumbar spine MRI: a prospective comparison with standard MRI. *Eur Radiol*. 2023;33(12):8656–8668.
4. **Choi Y-S**. Pathophysiology of degenerative disc disease. *Asian Spine J*. 2009;3(1):39–44.
5. **Maher C**, **Underwood M**, **Buchbinder R**. Non-specific low back pain. *Lancet*. 2017;389(10070):736–747.
6. **Priyadarshani P**, **Li Y**, **Yao L**. Advances in biological therapy for nucleus pulposus regeneration. *Osteoarthr Cartil*. 2016;24(2):206–212.
7. **Zhu J**, **Xia K**, **Yu W**, **et al**. Sustained release of GDF5 from a designed coacervate attenuates disc degeneration in a rat model. *Acta Biomater*. 2019;86:300–311.
8. **Zhang W**, **Li G**, **Luo R**, **et al**. Cytosolic escape of mitochondrial DNA triggers cGAS-STING-NLRP3 axis-dependent nucleus pulposus cell pyroptosis. *Exp Mol Med*. 2022;54(2):129–142.
9. **Zhao Y**, **Qiu C**, **Wang W**, **et al**. Cortistatin protects against intervertebral disc degeneration through targeting mitochondrial ROS-dependent NLRP3 inflammasome activation. *Theranostics*. 2020;10(15):7015–7033.
10. **Miller WP**, **Sha CM**, **Sunilkumar S**, **et al**. Activation of disulfide redox switch in REDD1 promotes oxidative stress under hyperglycemic conditions. *Diabetes*. 2022;71(12):2764–2776.
11. **Stevens SA**, **Gonzalez Aguiar MK**, **Toro AL**, **et al**. PERK/ATF4-dependent expression of the stress response protein REDD1 promotes proinflammatory cytokine expression in the heart of obese mice. *Am J Physiol Endocrinol Metab*. 2023;324(1):E62–E72.
12. **Pérez-Sisqués L**, **Solana-Balaguer J**, **Campoy-Campos G**, **et al**. RTP801/REDD1 is involved in neuroinflammation and modulates cognitive dysfunction in Huntington's disease. *Biomolecules*. - 2021;12(1):34.
13. **Gao C**, **Wang R**, **Li B**, **et al**. TXNIP/Redd1 signalling and excessive autophagy: a novel mechanism of myocardial ischaemia/reperfusion injury in mice. *Cardiovasc Res*. 2020;116(3):645–657.
14. **Alvarez-Garcia O**, **Matsuzaki T**, **Olmer M**, **Plate L**, **Kelly JW**, **Lotz MK**. Regulated in development and DNA damage response 1 deficiency impairs autophagy and mitochondrial biogenesis in articular cartilage and increases the severity of experimental osteoarthritis. *Arthritis Rheumatol*. 2017;69(7):1418–1428.
15. **Caplen NJ**, **Mousses S**. Short interfering RNA (siRNA)-mediated RNA interference (RNAi) in human cells. *Ann N Y Acad Sci*. 2003;1002:56–62.

16. **Alshaer W**, **Zureigat H**, **Al Karaki A**, **et al**. siRNA: Mechanism of action, challenges, and therapeutic approaches. *Eur J Pharmacol*. 2021;905: 174178.
17. **Chen J**, **Zhu H**, **Zhu Y**, **et al**. Injectable self-healing hydrogel with siRNA delivery property for sustained STING silencing and enhanced therapy of intervertebral disc degeneration. *Bioact Mater*. 2022;9:29–43.
18. **Chen S**, **Lei L**, **Li Z**, **et al**. Grem1 accelerates nucleus pulposus cell apoptosis and intervertebral disc degeneration by inhibiting TGF-β-mediated Smad2/3 phosphorylation. *Exp Mol Med*. 2022;54(4):518–530.
19. **Yonezawa S**, **Koide H**, **Asai T**. Recent advances in siRNA delivery mediated by lipid-based nanoparticles. *Adv Drug Deliv Rev*. 2020;154–155:64–78.
20. **Amiri A**, **Barreto G**, **Sathyapalan T**, **Sahebkar A**. siRNA therapeutics: future promise for neurodegenerative diseases. *Curr Neuropharmacol*. 2021;19(11):1896–1911.
21. **Caillaud M**, **Gobeaux F**, **Hémadi M**, **et al**. Supramolecular organization and biological interaction of squalenoyl siRNA nanoparticles. *Int J Pharm*. 2021;609:121117.
22. **Lv H**, **Zhang S**, **Wang B**, **Cui S**, **Yan J**. Toxicity of cationic lipids and cationic polymers in gene delivery. *J Control Release*. 2006;114(1):100–109.
23. **Reymond J-L**, **Bergmann M**, **Darbre T**. Glycopeptide dendrimers as Pseudomonas aeruginosa biofilm inhibitors. *Chem Soc Rev*. 2013;42(11): 4814–4822.
24. **van Dongen MA**, **Vaidyanathan S**, **Banaszak Holl MM**. PAMAM dendrimers as quantized building blocks for novel nanostructures. *Soft Matter*. 2013;9(47):9.
25. **Fox LJ**, **Richardson RM**, **Briscoe WH**. PAMAM dendrimer - cell membrane interactions. *Adv Colloid Interface Sci*. 2018;257:1–18.
26. **Bai S**, **Thomas C**, **Ahsan F**. Dendrimers as a carrier for pulmonary delivery of enoxaparin, a low-molecular weight heparin. *J Pharm Sci*. 2007;96(8):2090–2106.
27. **Soydan Z**, **Bayramoglu E**, **Urut DU**, **Iplikcioglu AC**, **Sen C**. Tracing the disc: the novel qualitative morphometric MRI based disc degeneration classification system. *JOR Spine*. 2024;7(1):e1321.
28. **World Medical Association**. World Medical Association Declaration of Helsinki: ethical principles for medical research involving human subjects. *JAMA*. 2013;310(20):2191–2194.
29. **He R**, **Wang Z**, **Cui M**, **et al**. HIF1A Alleviates compression-induced apoptosis of nucleus pulposus derived stem cells via upregulating autophagy. *Autophagy*. 2021;17(11):3338–3360.
30. **Shen J**, **Fang J**, **Hao J**, **et al**. SIRT1 inhibits the catabolic effect of IL-1β through TLR2/SIRT1/NF-κB pathway in human degenerative nucleus pulposus cells. *Pain Physician*. 2016;19(1):E215–26.
31. **Chen C-J**, **Zhao Z-X**, **Wang J-C**, **et al**. A comparative study of three ternary complexes prepared in different mixing orders of siRNA/redox-responsive hyperbranched poly (amido amine)/hyaluronic acid. *Int J Nanomedicine*. 2012;7:3837–3849.
32. **Bai Z**, **Shou Z**, **Hu K**, **Yu J**, **Meng H**, **Chen C**. Melatonin protects human nucleus pulposus cells from pyroptosis by regulating Nrf2 via melatonin membrane receptors. *Bone Joint Res*. 2023;12(3):202–211.
33. **Bahar ME**, **Hwang JS**, **Ahmed M**, **et al**. Targeting autophagy for developing new therapeutic strategy in intervertebral disc degeneration. *Antioxidants (Basel)*. 2022;11(8):11.
34. **Wang W-J**, **Yu X-H**, **Wang C**, **et al**. MMPs and ADAMTSs in intervertebral disc degeneration. *Clin Chim Acta*. 2015;448:238–246.
35. **Yin H**, **Wang K**, **Das A**, **et al**. The REDD1/TXNIP complex accelerates oxidative stress-induced apoptosis of nucleus pulposus cells through the mitochondrial pathway. *Oxid Med Cell Longev*. 2021;2021:7397516.
36. **del Olmo-Aguado S**, **Núñez-Álvarez C**, **Ji D**, **Manso AG**, **Osborne NN**. RTP801 immunoreactivity in retinal ganglion cells and its down-regulation in cultured cells protect them from light and cobalt chloride. *Brain Res Bull*. 2013;98:132–144.
37. **Szklarczyk D**, **Gable AL**, **Nastou KC**, **et al**. The STRING database in 2021: customizable protein-protein networks, and functional characterization of user-uploaded gene/measurement sets. *Nucleic Acids Res*. 2021;49(D1):D605–D612.
38. **Stelzer G**, **Rosen N**, **Plaschkes I**, **et al**. The genecards suite: from gene data mining to disease genome sequence analyses. *Curr Protoc Bioinformatics*. 2016;54:1.
39. **Bu D**, **Luo H**, **Huo P**, **et al**. KOBAS-i: intelligent prioritization and exploratory visualization of biological functions for gene enrichment analysis. *Nucleic Acids Res*. 2021;49(W1):W317–W325.
40. **Li J**, **Liang H**, **Liu J**, **Wang Z**. Poly (amidoamine) (PAMAM) dendrimer mediated delivery of drug and pDNA/siRNA for cancer therapy. *Int J Pharm*. 2018;546(1–2):215–225.
41. **Tarach P**, **Janaszewska A**. Recent advances in preclinical research using PAMAM dendrimers for cancer gene therapy. *Int J Mol Sci*. - 2021;22(6):2912.
42. **Masuda K**, **Imai Y**, **Okuma M**, **et al**. Osteogenic protein-1 injection into a degenerated disc induces the restoration of disc height and structural changes in the rabbit anular puncture model. *Spine (Phila Pa 1976)*. 2006;31(7):742–754.
43. **Yin H**, **Zhang Y**, **Wang K**, **et al**. The involvement of regulated in development and DNA damage response 1 (REDD1) in the pathogenesis of intervertebral disc degeneration. *Exp Cell Res*. 2018;372(2):188–197.
44. **Zhou Z**, **Fan Y**, **Zong R**, **Tan K**. The mitochondrial unfolded protein response: a multitasking giant in the fight against human diseases. *Ageing Res Rev*. 2022;81:101702.
45. **Nicholls DG**, **Budd SL**. Mitochondria and neuronal survival. *Physiol Rev*. 2000;80(1):315–360.
46. **Dan Dunn J**, **Alvarez LA**, **Zhang X**, **Soldati T**. Reactive oxygen species and mitochondria: a nexus of cellular homeostasis. *Redox Biol*. 2015;6: 472–485.
47. **Borowiec AM**, **Właszczuk A**, **Olakowska E**, **Lewin-Kowalik J**. TXNIP inhibition in the treatment of diabetes. Verapamil as a novel therapeutic modality in diabetic patients. *Med Pharm Rep*. 2022;95(3):243–250.
48. **Chang H**, **Cai F**, **Zhang Y**, **et al**. Silencing gene-engineered injectable hydrogel microsphere for regulation of extracellular matrix metabolism balance. *Small Methods*. 2022;6(4):e2101201.
49. **Dogbey DM**, **Torres VES**, **Fajemisin E**, **et al**. Technological advances in the use of viral and non-viral vectors for delivering genetic and non-genetic cargos for cancer therapy. *Drug Deliv Transl Res*. 2023;13(11): 2719–2738.
50. **Chauhan AS**. Dendrimers for drug delivery. *Molecules*. 2018;23(4):23.
51. **Navath RS**, **Menjoge AR**, **Wang B**, **Romero R**, **Kannan S**, **Kannan RM**. Amino acid-functionalized dendrimers with heterobifunctional chemoselective peripheral groups for drug delivery applications. *Biomacromolecules*. 2010;11(6):1544–1563.
52. **Nam HY**, **Hahn HJ**, **Nam K**, **et al**. Evaluation of generations 2, 3 and 4 arginine modified PAMAM dendrimers for gene delivery. *Int J Pharm*. 2008;363(1–2):199–205.
53. **Wang M**, **Cheng Y**. Structure-activity relationships of fluorinated dendrimers in DNA and siRNA delivery. *Acta Biomater*. 2016;46:204–210.
54. **Choi KY**, **Han HS**, **Lee ES**, **et al**. Hyaluronic acid-based activatable nanomaterials for stimuli-responsive imaging and therapeutics: beyond CD44-mediated drug delivery. *Adv Mater*. 2019;31(34):e1803549.
55. **Han M**, **Lv Q**, **Tang X-J**, **et al**. Overcoming drug resistance of MCF-7/ADR cells by altering intracellular distribution of doxorubicin via MVP knockdown with a novel siRNA polyamidoamine-hyaluronic acid complex. *J Control Release*. 2012;163(2):136–144.
56. **Zhang X**, **Pan J**, **Yao M**, **et al**. Charge reversible hyaluronic acid-modified dendrimer-based nanoparticles for siMDR-1 and doxorubicin co-delivery. *Eur J Pharm Biopharm*. 2020;154:43–49.
57. **Fraser JRE**, **Laurent TC**, **Laurent UBG**. Hyaluronan: its nature, distribution, functions and turnover. *J Intern Med*. 1997;242(1):27–33.
58. **Piras M**, **Fanni D**, **Congiu T**, **et al**. CD44 is highly expressed in stem/progenitor cells originating the intervertebral discs in the human notochord. *Eur Rev Med Pharmacol Sci*. 2022;26(22):8502–8507.
59. **Leiro V**, **Garcia JP**, **Moreno PMD**, **et al**. Biodegradable PEG-dendritic block copolymers: synthesis and biofunctionality assessment as vectors of siRNA. *J Mater Chem B*. 2017;5(25):4901–4917.

Author information

M. Ma, MD, Orthopaedic Surgeon
X. He, MD, Orthopaedic Surgeon
D. Zhu, MD, Orthopaedic Surgeon
X. Kang, MD, Orthopaedic Surgeon

The Second Clinical Medical College, Lanzhou University, Lanzhou, China; Department of Orthopaedics, Lanzhou University Second Hospital, Lanzhou, China.

C. Zhang, MD, Orthopaedic Surgeon, Department of Sports Medicine, The Second Affiliated Hospital of Fujian Traditional Chinese Medical University, Fuzhou, China.

Z. Zhong, MD, Orthopaedic Surgeon, Department of Orthopaedics, Ruijin Hospital, Shanghai Jiao Tong University, Shanghai, China.

Y. Wang, MD, Surgical Oncologist, Department of Oncology, Zhangye People's Hospital Affiliated to Hexi University, Zhangye, China.

Z. Qian, MD, Orthopaedic Surgeon, Department of Joint and Sports Medicine, Institute of Orthopaedic Diseases, Zhangye People's Hospital Affiliated to Hexi University, Zhangye, China.

B. Yu, MD, Orthopaedic Surgeon, Shanghai Seventh People's Hospital, Shanghai University of Traditional Chinese Medicine, Shanghai, China.

Author contributions

M. Ma: Investigation, Methodology, Writing – original draft.
C. Zhang: Methodology, Formal analysis.
Z. Zhong: Investigation, Methodology.
Y. Wang: Formal analysis.
X. He: Visualization.
D. Zhu: Visualization.
Z. Qian: Conceptualization, Resources, Funding acquisition.
B. Yu: Conceptualization, Resources.
X. Kang: Conceptualization, Resources, Writing – review & editing, Funding acquisition.

M. Ma, C. Zhang, and Z. Zhong contributed equally to this work.

Funding statement

The authors disclose receipt of the following financial or material support for the research, authorship, and/or publication of this article: this work was supported by the National Natural Science Foundation of China (82272536), Gansu Provincial University Youth Doctoral Fund Project (2022QB-160), and Gansu Provincial University Innovation Fund Project (2022A-121).

ICMJE COI statement

The authors disclose receipt of the following financial or material support for the research, authorship, and/or publication of this article: this work was supported by the National Natural Science Foundation of China (82170897, 82272536), Gansu Provincial University Youth Doctoral Fund Project (2022QB-160), and Gansu Provincial University Innovation Fund Project (2022A-121).

Data sharing

All data generated or analyzed during this study are included in the published article and/or in the supplementary material.

Acknowledgements

We thank Bullet Edits Limited for the linguistic editing and proofreading of the manuscript.

Ethical review statement

The study was performed in accordance with the 1964 Declaration of Helsinki and subsequent versions, and was approved by The Human Ethics Committee of Lanzhou University Second Hospital (2023A-105) and The Animal Ethics Committee of the Lanzhou University Second Hospital (D2023-145). All enrolled patients provided written informed consent and all animal experiments were conducted in accordance with the National Institutes of Health (NIH, USA) Guide for the Care and Use of Laboratory.

Open access funding

This work was supported by the National Natural Science Foundation of China (82272536).